UW Journal of Science and Technology Vol. 6 (2022) 45-53
ISSN: 2523-0123 (Print) 2616-4396 (Online)

University of Wah
Journal of Science and Technology

www.uow.edu.pk

A Comparative Analysis of Artificial Intelligence and Machine learning Approach to Estimate Currents in Electrical Power Transmission Lines

Haseeb Javed, Muhammad Shahzad Pansota, Hamza Ali Khan and Ali Rehman

***Abstract*—Using pyro-sensors, machine learning (ML) methods, and artificial intelligence, this suggested study enlightens an idea to monitor current in high voltage transmission lines. Data can be collected in the form of heat waves (infrared waves) created by the electric current in the transmission/distribution line using pyro-sensors installed around the transmission/distribution lines. The suggested approach processes this data using a neural network-based artificial intelligence algorithm to determine the transmission line's current. MATLAB simulation neural network toolkit is used to test and validate the suggested technique's validity with backward forwarding propagation (FFBP) type and with feed-forward distributed time delay (FFDTD) and compare it to get the best validation performance for the proposed approach. It is validated that feed-forward distributed time delay (FFDTD) gives the best validation performance (0.98256) at epoch 0 as compared to the forward, backward propagation (FFBP), which offers the best validation performance at (1.984), it means validation performance of FFDTD is better than FFBP. It also tells us that these simulation findings compare projected current to actual current, implying that the existing CT current measuring technology at the grid station may be replaced.**

***Index Terms* — Pyro-sensors, Artificial Intelligence, Current transformer, Machine learning, Potential transformer.**

I. Introduction

THE community's ever-increasing need for electric power supply necessitates concerted measures to maintain grid stations operational around the clock. The frequency, current, and phase of high-voltage power lines are critical indicators of power transmission quality.

Manuscript received; Sep 17, 2021; accepted Dec 27, 2021.

H. Javed (email: haseebjaved1996@yahoo.com), M.S. Pansota (e-mail: shahzadpansota@hotmail.com), H.A. Khan (email:hamzaalikhanleo@gmail.com) and A. Rehman (email:rehman.alirehman@gmail.com) are affiliated with Department of Electrical Engineering, Muhammad Nawaz Sharif University of Engineering & Technology, Multan 60000, Pakistan.

*Corresponding authors: e-mail: haseebjaved1996@yahoo.com

As a result, it is critical to continually create and send these values through high power transmission lines. It is also critical to monitor the real-time quality of electricity transferred via high-voltage transmission lines located distant from power plants and substations. No intelligent technology is available to assess power line quality in any distant site [1], [2]. The typical measuring technique comprises a contact current transformer (CT) at the end of a transmission line [3]; however, CT cannot measure power quality or other characteristics at a specific point in high voltage transmission lines. Furthermore, the contact measuring method has numerous safety and electrical damage issues due to the electromagnetic fields produced on the conductors. Noncontact measuring techniques are used to measure the current, voltage, and frequency of high-power lines, and when discussing noncontact measurement phenomena, temperature measurement techniques appear to be very trustworthy since they are extensively employed in a variety of applications in recent days. Several temperature measuring techniques are mentioned below.

Temperature is the most common and important physical property that is measured. As a result, sensor usage has a wide variety of applications and accounts for a sizable portion of the sensor market in terms of volume [4]. Multiple physical elements being detected and quantified (e.g., humidity, pressure, motion, body temperature, flow, stress, and gas concentration) revolve around temperature swings, therefore temperature changes must be compensated [5]. Several temperature sensing methods, such as thermal expansion [6], thermoelectricity [7], fluorescence [8], and others, are in use and are based on vivid physical phenomena.

Temperature measuring techniques are classified into three types based on their relative location in relation to the environment [6]. I Invasive: When the sensor is in direct contact with the medium of interest (for example, a thermocouple in a gas stream), ii) Semi-Invasive: In some

systems, the medium of interest behaves to produce remote outputs (for example, surface coatings whose colour changes with temperature), iii) Non-Invasive: The medium of interest is monitored remotely (e.g., IR thermography). Because a non-contact (non-invasive) temperature measuring technique employs an infrared (IR) sensor, it is necessary to explain remote monitoring IR technology before proceeding. Since the discovery of the invisible spectrum, the use of infrared sensors has skyrocketed. The invisible spectrum is not visible to the naked eye, but it may be detected by the amount of heat emitted by the light.

Thermal sensors/IR thermometers are becoming increasingly important in order to see and explain this invisible spectrum. Radiation thermometers detect the heat radiation emitted from a material's surface. The infrared ray is a longer wavelength electromagnetic wave. The wavelength of infrared radiation ranges from 0.75m to 1m [9]. When compared to its absolute temperature ratings, all matter emits thermal radiation or heat energy [10]. Spans from gamma rays to microwaves with wavelengths ranging from 10-12m to hundreds of meters, encompassing x rays, UV rays, visible spectrum, and infrared waves in between two extremes. Such critical information is required to comprehend the impetus for replacing present voltage measurement technology PTs with the IR temperature sensor. But first, let's look at some of the disadvantages of utilizing PTs at grid stations.

Overhead transmission cables must be monitored to ensure a continuous power supply across vast distances. Fault occurrence is likely in overhead transmission lines, which might produce sudden changes in voltage and frequency amplitude [11]. In addition, specific renewable energy sources may produce power variations and voltage changes [12]. Furthermore, sectional monitoring is required for these high-power transmission lines since they cover a vast geographical region and are subjected to a variety of environmental conditions. For example, if an event occurs at a specific place, remedial actions such as disconnecting and reconnecting should be performed as soon as possible to alleviate the cause. Large frequency bandwidth should also be addressed, as it is a fundamental need of newly built high-voltage DC transmission grids [13]. Furthermore, traditional potential transformers (PT) cannot fulfil these measurement criteria [14] because magnetic core problems in PTs limit the frequency bandwidth in the tens of Hz to kHz range. Given the high cost of PTs' ferromagnetic material and the required galvanic connection to high-voltage live wires, PTs are unlikely to be deployable to cover broad geographical areas for divisional monitoring. To discover an inexpensive and effective solution, researchers are looking for new avenues of current and voltage measurements, like as:

- Numerous academic attempts are being undertaken to build a smart system for monitoring the power for overhead transmission lines from any remote place [10].
- One study [15] is presented in the literature that emphasizes the capability of microprocessors for data collecting and processing based on hall sensing theory.
- In the literature [16], a noncontact measuring system is designed using a CT voltage sensor and wireless transmission technology.
- Another approach described in [17] is the use of capacitive coupling with magnetic field sensing to detect non-contact voltages of overhead transmission lines that cover a broad geographical region.

The use of infrared sensors has skyrocketed since the discovery of the invisible spectrum. The invisible spectrum is not visible to the naked eye, but it may be detected by the amount of heat produced by light. Thermal sensors/IR thermometers are becoming increasingly important for seeing and communicating this unseen spectrum. Radiation thermometers detect the heat radiation emitted by a material's surface. The infrared ray is an electromagnetic wave with a longer wavelength. The wavelength of infrared light ranges from 0.75m to 1m [9]. Every substance emits thermal radiation or heat energy in proportion to its absolute temperature [10]. The suggested study's blueprint includes a PIR (pyroelectric infrared) detecting module, which serves as the proposed system's backbone and is linked to a high-power transmission line above. The suggested heatwave measurement system is depicted in *Fig. 1*, and the component details are discussed further below. At non-zero temperatures, all matter emits radiation, some visible and some invisible, such as ultraviolet UV rays and infrared IR.

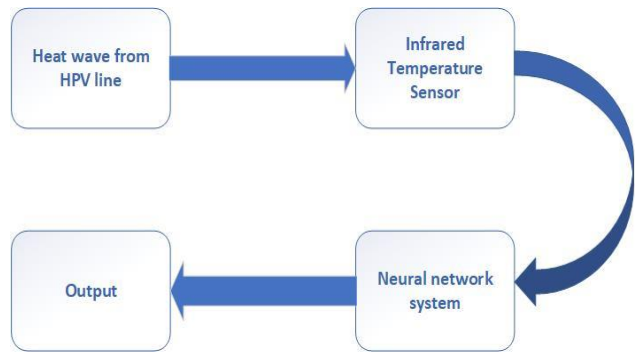

Fig. 1. Proposed structure of heat-wave measurement system, it shows that the temperature sensor detects heat waves emitted by above power lines. The optimum distance between the IR sensor and the measuring item is determined by the IR temperature sensor standard. This measurement values will then be transmitted to an analogue to digital converter, which will then transmit digital output to an artificial intelligent network.

II. HEAT WAVES OR THERMAL RADIATION

The wavelength range of thermal radiation of heat waves produced by all stuff at zero temperature is 0.1 m to 100 m. *Fig. 2*, depicts several areas of the electromagnetic spectrum, as well as the ranges of each zone. The phenomenon of generating radiation from matter is caused by collisions of matter electrons, which release energy. Because thermal radiations are likewise electromagnetic,

the propagation characteristics of electromagnetic waves may be applied to them [18], [19]. The relationship between frequency and wavelength of thermal radiations may be expressed as =c/v, where c is the speed of light, 2.998108 m/s.

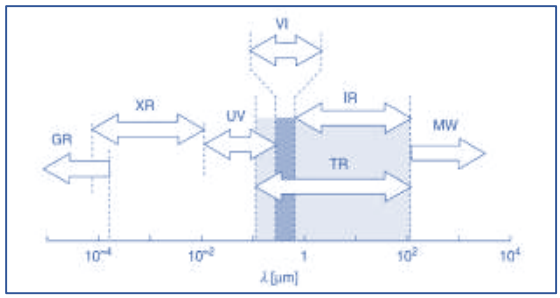

Fig. 2. Electromagnetic Spectrum (XR X-rays; GR gamma rays; UV ultraviolet; MW microwaves; IR infrared; VI visible; TR thermal radiation;). It also shows depicts several areas of the electromagnetic spectrum, as well as the ranges of each zone.

III. TEMPERATURE MEASUREMENT SYSTEM DESIGN

The heat radiations released are non-directed and can be transferred in all directions of the conductor. An infrared temperature sensor can be installed here to record and analyse the emitted radiations from the high-power transmission lines to monitor current, voltage, and frequency. The IR temperature sensor is explained more below. Given the length of the insulators normally attached to the tower, the minimum distance should be about 1cm, and the spot size at that distance should not be larger than 3 cm given the size of the attached sphere. The minimum temperature for the transmission conductor depends on the material used, but it is common to specify the temperature range of the conductor from 50 C to 70 C as the maximum operating temperature so that the required temperature range could vary from a few degrees Celsius to nearly one hundred Celsius depending on the weather conditions, cold or hot.

The heatwave measuring system is made up of two major components: an infrared thermometer and a nonconducting shell in which the pyro-sensor is inserted to achieve a non-contact system [20]. To select the thermometer, three factors were available: cost, spot size, and, most significantly, temperature range.

Price was also a significant and essential factor in creating and implementing this concept in order to create a viable alternative to existing contact temperature monitoring devices, which cost several thousand dollars. *Fig. 3*, depicts a simplified block diagram of a non-contact temperature measurement sensor. The power line temperature is determined by the quantity of heat generated by the high transmission lines. At room temperature, there will be relatively few photons released from the surface of the transmission line, and the number of photons emitted will stay low until the temperature of the surface exceeds a particular threshold value. Once the conductor's surface is heated enough to break the threshold point, an excess of photons will be released from the conductor, generating a noticeable number of heatwaves for the IR sensor.

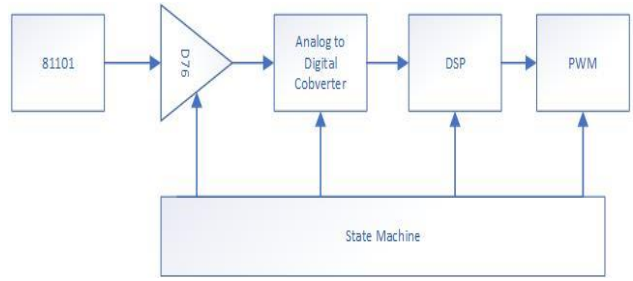

Fig. 3. Temperature Sensor Block diagram. It shows a simplified block diagram of a non-contact temperature measurement sensor with many connected blocks are explained below.

Since heat is a kind of energy (E) and assuming the conductor current, resistance, and length of time the current flows through the conductor are known, the quantity of heat may be estimated as follows:

$$P = W/t \Rightarrow E/t \quad (1)$$

$$E = Pt \Rightarrow I^2Rt \quad (2)$$

$$H = I^2Rt \quad (3)$$

Now, in order to elaborate on the suggested current measurement approach, the following key components of the heatwave measuring device are described in detail:

A. Thermopile Sensor (81101)

The non-contact temperature sensor 81101 was chosen as the infrared sensor for this investigation. It may be used to measure component temperatures and body temperature, surface temperature, heat ventilation, and much more. This IR sensor has a temperature range of 40°C to 125°C, a spectral range of 8 m to 14 m, and a measurement resolution of 0.02°C.

This non-contact temperature measurement sensor operates on the thermocouple concept, in which heat waves from high-power transmission lines are detected and transformed to electrical signals for further processing. The thermopile sensors are made using several polysilicon technologies [21], [22], as well as Bi-Sb-Te [23].

B. Amplifier

The goal is to enhance the signal received from the IR sensor, which may be quite faint in reality. As previously stated, Plank's law may represent thermal radiation emitted by heated surfaces, which states that radiance rises exponentially with (absolute) temperature. To maximize the gain of the recorded heatwave signal, a band-pass amplifier with a total gain of 1000 might be employed. Furthermore, the amplifier must be quick (high bandwidth), low-noise, linear, and capable of performing across a wide dynamic range [24][25]. The boosted signal is then supplied into an A/D converter. iii). A/D Converter

C. A/D Converter

The three fundamental processes for converting an analog signal to a digital signal are sampling, quantization,

and coding. The nature of the signal changes after going through the A/D converter since our ultimate aim is additional digital signal processing at the neural network end to estimate the current and voltage values of the high-power transmission.

The equation to compute the output for a single layer ANN network with three inputs (x1, x2, and x3) and three weights (w1, w2, and w3) and a bias (b) related to information storage may be seen in *Fig. 4.* lines. A state machine governs the functioning of the temperature sensor, which regulates the measurement and determines the object's air temperature. PWM then outputs this post-processing of the measured temperature. The following is a brief description of the sensor components of temperature.

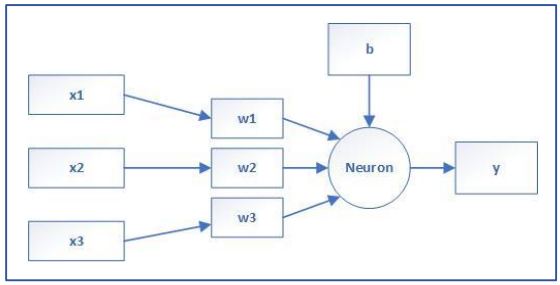

Fig. 4. Single layer Artificial neural network architecture. It computes the output for a single layer ANN network with three inputs (x1, x2, and x3) and three weights (w1, w2, and w3) and a bias (b) related to information storage.

IV. Artificial Neural Network (ANN)

The discovery of a neuron in the human brain throughout the nineteenth century opened up new avenues for scientists and researchers to investigate the phenomenon. This biological discovery also transformed the electronics sector, and artificial neural networks (ANN) research is eerily similar to human neurons. It is estimated that the human brain has around 85 billion neurons [26], and ANN functions in a way similar to that of the human brain. Different neurons in an ANN network are linked together by weights.

ANN networks are remarkable in their ability to forecast or estimate system values and learn and emphasize the correlation between system parameters. The workings of ANN are described in detail in the literature [27].

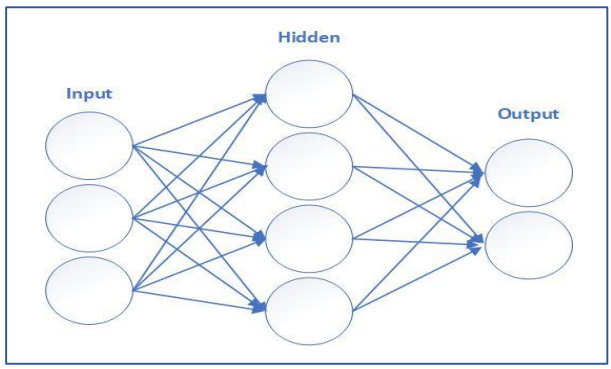

Fig. 5. Single artificial neural network (ANN) node. A typical ANN network architecture includes many layers and nodes. Depending on the needs of the operation, ANN systems can be single or multilayer. The element that can gather information and conduct simple actions is the node, which mimics organic neurons. This information is then distributed to various neurons/nodes. The activation value of each node is its output.

Fig. 5 depicts a single-layer ANN system with several nodes.

$$o = (w1 * x1) + (w2 * x2) + (w3 * x3) + b \quad (4)$$

From (4), w = [$w1\ w2\ w3$] and x = [$x1\ x2\ x3$] Where is an activation function; thus the output of a neural network node may be represented as and can be seen in *Fig. 5*:

$$y = \varphi(o) = \varphi(wx + b) \quad (5)$$

where o = $(wx + b)$ and is a typical step or linear function, known as the activation function for an ANN system, that affects the behaviour of a node. This transfer function, which is based on the input and output layers, also indicates the system's predicted output. Whereas bias (b) is an offset of a neuron's threshold value and is frequently envisioned as a feature of the activation function.

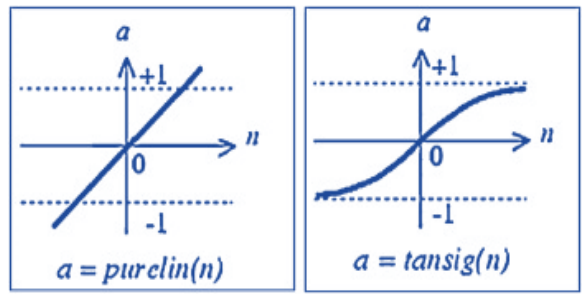

Fig. 6. Multiple Unit Activation Functions. Fig. 6 (a), Fig 6 (b) The linear activation function is simpler to comprehend, but it can only be used for a single layer neural network as (x) = x, as illustrated in Fig. 6 (a). Whereas bias (b) is an offset of a neuron's threshold value and is frequently envisioned as a feature of the activation function.

There are two types of activation functions used: linear and sigmoid. The linear activation function is simpler to comprehend, but it can only be used for a single layer neural network as (x) = x, as illustrated in *Fig. 6 (a)*, because all hidden layers become useless for this function.

The bias value serves as a reference point against which the inputs may be evaluated in order to create output. If the input values are less than the biased value, the sigmoid function is used.

The sigmoid function, shown in *Fig. 6 (b)*, is a smooth limiting function with the mathematical representation:

$$f(x) = 1/(1 - exp - x) \quad (6)$$

A. Feed forward Back Prop (FFBP) Testing

A rapid feed forward-backwards propagation (FFBP) type is utilized for training a neural network for incoming data to anticipate an approximated output. The training of a neural network is based on splitting the data (voltage or current waves from PWM) into three sets: the training set, the validating set, and the testing set, which are used to test the efficiency of neural networks. Using the MATLAB Neural Network toolbox [28], such dynamic artificial neural networks may be converted to open or closed-loop

networks. *Fig. 7*, depicts a block schematic of the system with progress validation.

The neural network was trained using the Levenberg Marquardt backpropagation method. Although it requires more memory than other algorithms (for example, Bayesian Regulation and Scaled Conjugate Radiant), it has high performance and is quick for training. The training function's divider and argument are used to split the data samples.

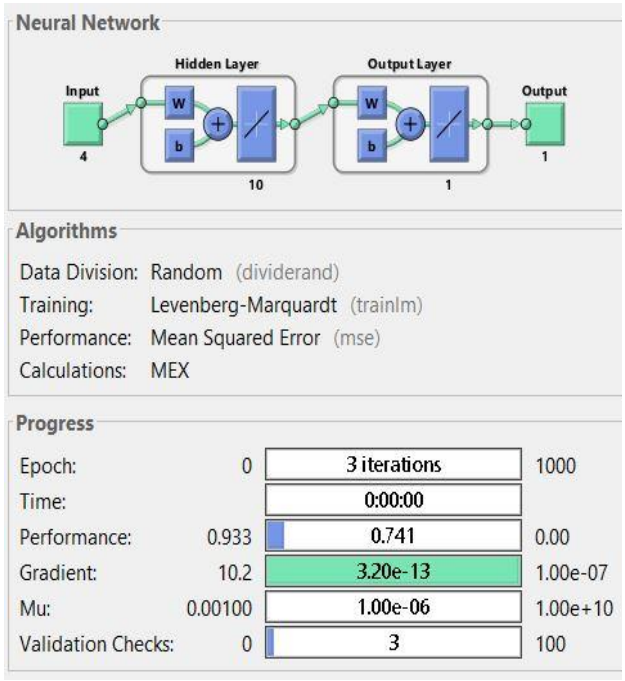

Fig. 7. Open-loop neural network progress validation (FFBP). Using the open-loop and closed-loop functions in the MATLAB Neural Network toolbox [28], such dynamic artificial neural networks may be converted to open or closed-loop networks.

As a result, 70% of the data samples are utilized for training, 15% for validation, and the remaining 15% are used to compare the output of the trained neural network to the actual output values. The forecasts' results are in close proximity to the original data collected from the power lines. *Fig. 8*, depicts the training performance and prediction results for N=100 samples using MATLAB. Four input values are used: maximum conductor temperature, minimum conductor temperature, output voltage or external ambient temperature, and noise. *Fig. 9 (a)* displays the best validation performance (1.984) at 0 epochs, while *Fig. 9(b)*, shows the regression values, indicating how effectively the neural network is trained as the Training R-value is almost equal to 1. *Fig. 9(c)* shows the validation checking of the given test.

Fig. 9(d), depicts the overlapping signals of real and anticipated data. (e) displaying the relatively low error signal between the actual and projected data, arguing for the system's efficiency in producing expected output.

B. *Feed forward distributed time delay (FFDTD) Testing*

A feed forward distributed time delay (FFDTD) is also utilized for training a neural network for incoming data to anticipate an approximated best required output again. The training of this neural network is also based on three sets: the training set, the validating set, and the testing set, which are used to test the better efficiency of neural networks. Using the open-loop and closed-loop functions in the MATLAB Neural Network toolbox [28], such dynamic artificial neural networks may also be converted to open or closed-loop networks.

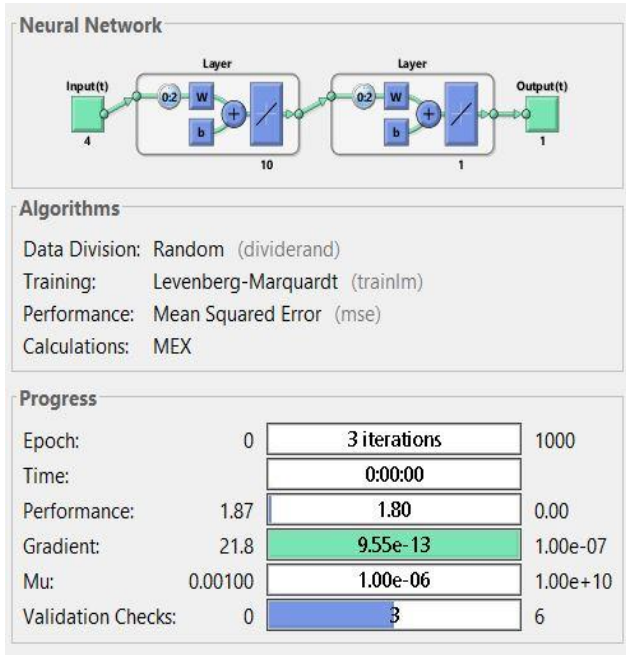

Fig. 8. Open-loop neural network progress validation (FFDTD). Using the open-loop and closed-loop functions in the MATLAB Neural Network toolbox [28], such dynamic artificial neural networks may be converted to open or closed-loop networks.

This neural network was also trained using the Levenberg Marquardt backpropagation method. Although it requires more memory than other algorithms (for example, Bayesian Regulation and Scaled Conjugate Radiant), it has high performance and is quick for training. The training function's divider and argument are used to split the data samples. *Fig. 10*, depicts a block schematic of the FFDTD system with the progress of the training validation.

As a result, *Fig. 10*, also depicts the training performance and prediction results for N=100 samples using MATLAB. Four input values are used: maximum conductor temperature, minimum conductor temperature, output voltage or external ambient temperature, and noise. *Fig. 10(a)*, displays the best validation performance (0.98256) at 0 epochs which is better as compared to the FFBP, while *Fig. 10(b)*, shows the predicted signal values. *Fig. 10(c)*, shows the validation checking of the given FFDTD model. *Fig. 10(d)*, displaying the relatively low error signal between the actual and projected data, arguing for the system's efficiency in producing the expected output.

Table I is the confirmation from which the data was predicted for N=100 samples with 20 neurons.

Feed forward back propagation (FFBP)

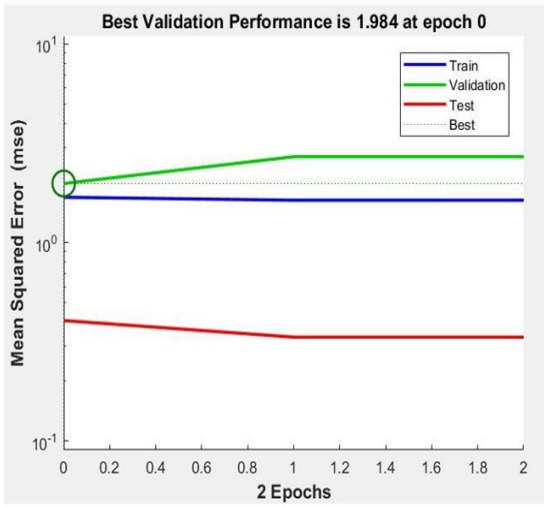

(a) The training Process

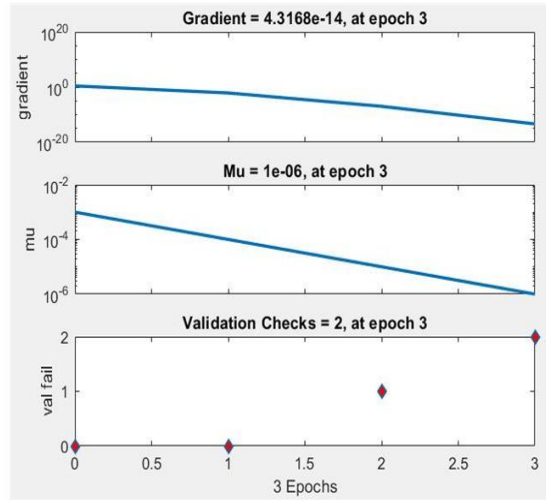

(c) Validation Checking

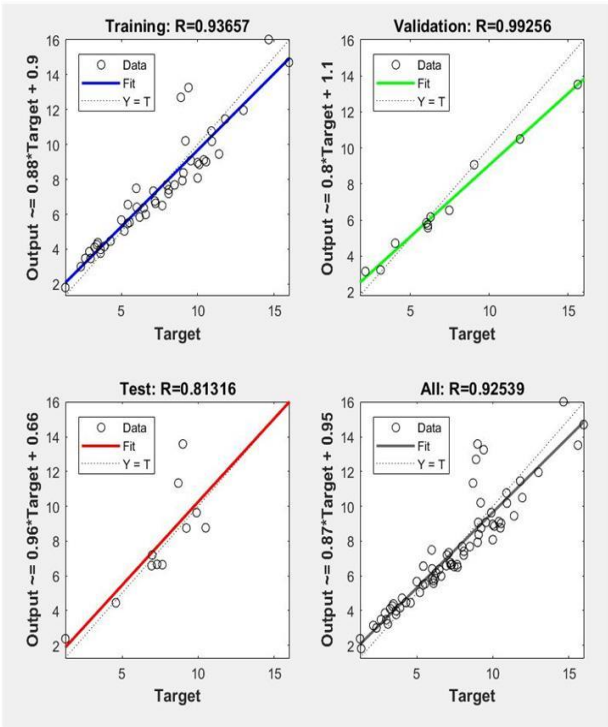

(b) The training Process

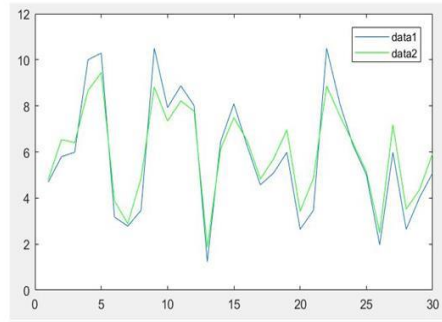

(d) Predicted Signal

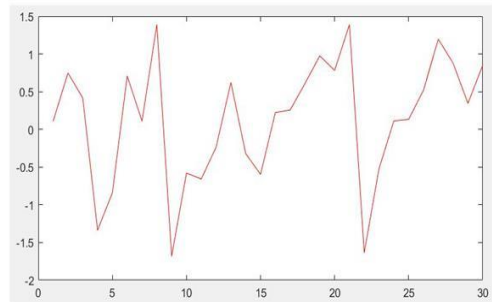

(e) Error Signal

Fig. 9.Validation ampacity results of prediction and training the power-transmission lines by FFBP.
Figure 9 (a) displays the best validation performance (1.984) at 0 epochs,
Figure 9 (b) shows the regression values, indicating how effectively the neural network is trained as the Training R-value is almost equal to 1.
Figure 9 (c) shows the validation checking of the given test.
Figure 9 (d) depicts the overlapping signals of real and anticipated data.
Figure (e) displaying the relatively low error signal between the actual and projected data, arguing for the system's efficiency in producing expected output

Feed forward Distributed Time Delay (FFDTD)

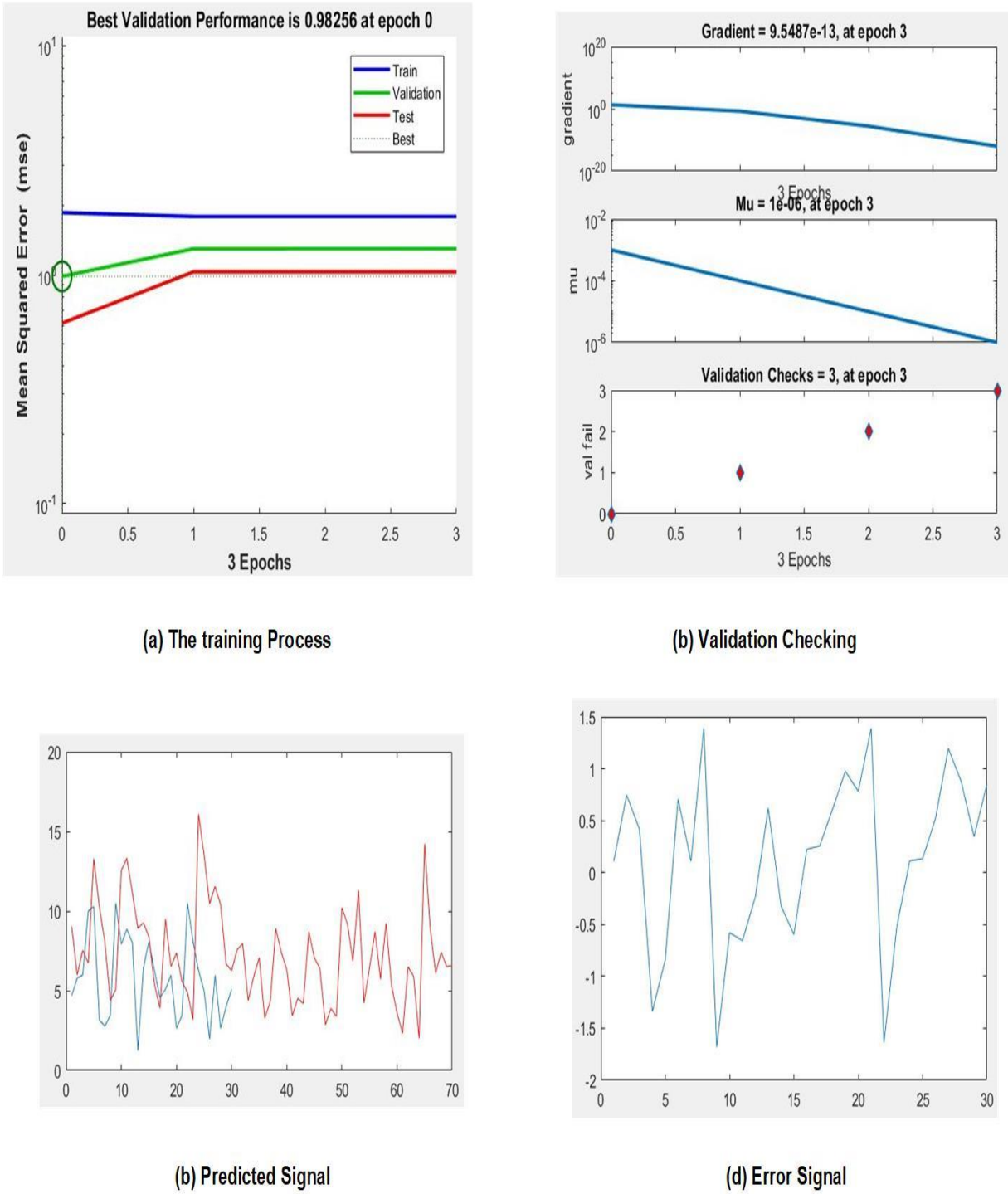

Fig. 9. Validation ampacity results of prediction and training the power-transmission lines by FFDTD.
Figure 10 (a) displays the best validation performance (0.98256) at 0 epochs which is better as compared to the FFBP, while Figure 10 (b) shows the predicted signal values. Figure 10 (c) shows the validation checking of the given FFDTD model. Figure 10 (d) displaying the relatively low error signal between the actual and projected data, arguing for the system's efficiency in producing expected output.

Table I is the confirmation from which the data was predicted for N=100 samples with 20 neurons.

TABLE 1.
CURRENT RATINGS ACTUAL VS PREDICTED FOR OVERHEAD POWER TRANSMISSION LINES

Conductor Temp. C (Max)	Conductor Temp. C (Min)	Noise (db)	Voltage heat waves (V)	(Actual) Current (I)	(Predicted) Current (I)
25.1	12.3	1.5	1.01	4.7	3.063722
26.5	11.5	1.92	0.6	5.8	6.40029
25.4	9	1.6	0.8	6	7.158542
26.7	10.8	1.71	0.7	10.01	8.548354
26.1	14.3	1.92	1.6	10.3	10.32167
27	13.9	2.91	1.2	3.18	2.505309
28.7	13.5	2.79	0.9	2.79	-2.0386
27.6	12.9	3.74	0.4	3.47	4.901967
29.9	14.6	3.25	0.5	10.51	11.74541
28.2	11.8	2.21	1.5	7.93	7.818101
29	12.1	1.35	1.6	8.88	9.658339
28.8	10.8	1.54	1.3	8.02	9.784303
27.6	11.4	1.69	1	1.25	8.8044
26.2	12.7	3.64	1.06	6.45	6.270811
28.7	13.4	2.89	0.94	8.1	7.90933
30	13.8	2.41	0.54	6.28	6.197219
28.8	11.8	2	0.32	4.58	2.755288
29.7	9.9	3.51	1.09	5.1	5.168805
26.4	9.5	2.29	0.67	5.99	8.918331
25.2	8.1	2.46	0.78	2.65	-3.24083
29.6	8.8	2.84	0.55	3.47	4.230294
27.2	12.6	2.67	0.46	10.51	9.958013
30.2	13.9	3.14	0.24	8.1	10.08269
25.1	14.3	2.34	1.98	6.28	4.495562
25.9	13.7	1.69	1.63	5.02	5.871411
27.1	11.5	1.81	1.21	1.98	0.535059
31.9	13.9	1.43	1.37	5.99	7.513291
30.5	8.2	1.78	1.2	2.65	3.664728
28.8	11.7	3.52	0.71	4.02	0.76287
25.2	9.1	3.47	0.64	5.1	5.07555

V. CONCLUSION

An approach for estimating current in high voltage transmission lines utilizing pyro-sensors, machine learning methods, and artificial intelligence is suggested in this work. On the collected data from high voltage power transmission lines, simulations using MATLAB software are run, and current estimation is computed using an artificial intelligence network method.

The suggested methodology's efficacy is validated by FFBP and FFDTD models using the MATLAB simulated neural network toolkit. It is validated that feed forward distributed time delay gives the best validation performance (0.98256) at epoch 0 as compared to the forward backward propagation which gives best validation performance at 1.984, it means validation performance of FFDTD is better than FFBP. Using pyro sensors and an ANN network, current estimates may be done in any remote place by tracing down existing power quality characteristics of high voltage power lines.

The positive findings for current predicted values are promisingly similar to actual current values, making the system trustworthy to use in the future as a substitute for CTs and PTs and may be used to measure current at any distant position on high power transmission.

REFERENCES

[1] Y. Wang, Z. Yang, H. Zhou, W. Cao, X. Yin, and Q. Guo. Study on transformer inrush current and CT saturation as well as the impact of their coupling effect on protection, IEEE Transportation Electrification Conference Expo, Asia-Pacific, 1, 2017.

[2] M. Kellermeier, C. Bert, and R. G. Müller. A novel concept for CT with fixed anodes (FACT): Medical imaging based on the feasibility of thermal load capacity, Physics Medica, vol. 31(5), pp. 425–434, 2015.

[3] J. Li and Y. Zhao. Co-simulation Research Based on Electromagnetic Induction of Wireless Power Transfer, 7th Int. Conf. Mechatronics, Computation, Education, Informationization (MCEI 2017), Vol. 75, pp. 577–580, 2018.

[4] J. Lorincz, I. Bule, and M. Kapov. Performance analyses of renewable and fuel power supply systems for different base station sites, Energies, Vol. 7(12), pp. 7816–7846, 2014..

[5] M. Mansoor, I. Haneef, S. Akhtar, A. De Luca, and F. Udrea. Silicon diode temperature sensors - A review of applications, Sensors Actuators, A Physics, vol. 232, pp. 63–74, 2015.

[6] P. R. N. Childs, J. R. Greenwood, and C. A. Long. Review of temperature measurement, *Review of Scientifc. Instrument*, Vol. 71(8), pp. 2959–2978, 2000.

[7] D. M. Nierman. Core temperature measurement in the intensive care unit, Critical Care Medicine, Vol. 19(6), pp. 818–823, 1991.

[8] A. Milewski, K. L. Ferguson, and T. E. Terndrup. Comparison of pulmonary artery, rectal, and tympanic membrane temperatures in

adult intensive care unit patients, Clinicalrics Pediatr, Vol. 30(4), pp. 13–17, 1991.

[9] E. B. Soyer. Pyroelectric Infrared Sensor Based Event Detection, Engineering, pp. 1–84, 2009.

[10] J. R. Howell and M. P. Mengüç. Challenges for radiative transfer 1: Towards the effective solution of conjugate heat transfer problems, Journal of Quantitative Spectroscopy and Radiative Transfer, Vol. 221, pp. 253–259, 2018.

[11] I. N. T. Lines. IEEE Transactions on Power Delivery, Vol. 3(1), pp. 288–297, 1988.

[12] J. M. Carrasco et al. Power-electronic systems for the grid integration of renewable energy sources: A survey, IEEE Transanctions on Industrial Electronics, Vol. 53(4), pp. 1002–1016, 2006,

[13] D. Jovcic, N. Pahalawaththa, and M. Zavahir. Analytical modelling of HVDC-HVAC systems, IEEE Transanctions on. Power Delivery, Vol. 14(2), pp. 506–511, 1999..

[14] M. Wang, A. J. Vandermaar, and K. D. Srivastava. Improved detection of power transformer winding movement by extending the FRA high frequency range, IEEE Transanctions on Power Delivery, Vol. 20(3), pp. 1930–1938, 2005.

[15] D. S. Pierce. A high precision non-contact gauge for distance measurement A high precision non-contact guage for distance measurement, 2016.

[16] T. Haiguo, Z. Jiran, G. Fangliang, L. Hua, F. Min, and H. Qi. Research on a rail-robot based remote three-dimensional inspection system for switch stations in power distribution network, Chinese Automation Congrress, Vol. 2017, pp. 7925–7930, 2017.

[17] K. Zhu, W. K. Lee, and P. W. T. Pong. Non-contact capacitive-coupling-based and magnetic-field-Sensing-assisted technique for monitoring voltage of overhead power transmission lines, IEEE Sensors Journals, Vol. 17(4), pp. 1069–1083, 2017.

[18] Z. Yanchao, J. Dong, K. Deshan, and C. Lin. Remote monitoring of power quality of high-voltage transmission lines, *IEEE International Conference on Electronics Measurement Instruments*, pp. 984–991, 2019.

[19] J. Meseguer, I. Pérez-Grande, and A. Sanz-Andrés. Thermal radiation heat transfer, Space Thermal Control, Vol. 2, pp. 73–86, 2012.

[20] P. Castro, R. Lecuna, M. Manana, M. J. Martin, and D. Del Campo. Infrared temperature measurement sensors of overhead power conductors, Sensors, Vol. 20(24), pp. 1–13, 2020.

[21] I. H. Choi and K. D. Wise. Silicon-thermopile-based infrared sensing array for use in automated manufacturing, IEEE Transactions Electronic Devices, vol. 33(1), pp. 72–79, 1986.

[22] R. Lenggenhager, H. Baltes, and T. Elbel. Thermoelectric infrared sensors in CMOS technology, Sensors Actuators A: Physics, Vol. 37–38, pp. 216-220, 1993.

[23] F. Völklein, A. Wiegand, and V. Baier. High-sensitivity radiation thermopiles made of BiSbTe films, Sensors Actuators A: Physics, Vol. 29(2), pp. 87–91, 1991.

[24] A. Dehé, K. Fricke, and H. L. Hartnagel. Infrared thermopile sensor based on AlGaAs—GasAs micromachining, Sensors and Actuators, A: Physical, Vol. 47(1-3), pp. 432–436, 1995.

[25] J. A. Young, S. Borror, A. W. Obst, J. R. Payton, and A. Seifter. Evaluation and comparison of three IR detectors and three amplifier designs for a new high-speed IR pyrometer, Ultrafast X-Ray Detectectors High-Speed Imaging and Applications, Vol. 5920, p. 592011, 2005.

[26] L. Chen, K. Sun, D. V. Shalashilin, M. F. Gelin, and Y. Zhao. Efficient simulation of time- And frequency-resolved four-wave-mixing signals with a multiconfigurational Ehrenfest approach, Journal of Chemical Physics, Vol. 154(5), 2021.

[27] S. A. Haider, S. R. Naqvi, T. Akram, and M. Kamran, Prediction of critical currents for a diluted square lattice using artificial neural networks, *Applied Sciience*, Vol. 7(3), 2017.

[28] A. Teymourifar. A comparison between two approaches to optimize weights of connections in artificial neural networks, Universse Journal of Applied Mathematics, Vol. 9(2), pp. 17–24, 2021..